University of Bath

Alternative formats
If you require this document in an alternative format, please contact:
openaccess@bath.ac.uk

Ratcheting droplet pairs

C. A. Galeano-Rios,[1, a)] M. M. P. Couchman,[2, b)] P. Caldairou,[2] and J. W. M. Bush[2, c)]

[1)]*Department of Mathematical Sciences, University of Bath, Bath, BA2 7AY,*
UK

[2)]*Department of Mathematics, Massachusetts Institute of Technology, Cambridge, MA 02139,*
USA

Millimetric droplets may be levitated on the surface of a vibrating fluid bath. Eddi *et al.*[1] demonstrated that when a pair of levitating drops of unequal size are placed nearby, they interact through their common wavefield in such a way as to self-propel through a ratcheting mechanism. We present the results of an integrated experimental and theoretical investigation of such ratcheting pairs. Particular attention is given to characterizing the dependence of the ratcheting behavior on the droplet sizes and vibrational acceleration. Our experiments demonstrate that the quantized inter-drop distances of a ratcheting pair depend on the vibrational acceleration, and that as this acceleration is increased progressively, the direction of the ratcheting motion may reverse up to four times. Our simulations highlight the critical role of both the vertical bouncing dynamics of the individual drops and the traveling wave fronts generated during impact on the ratcheting motion, allowing us to rationalize the majority of our experimental findings.

We consider droplet pairs of unequal size bouncing on the surface of a vibrating bath. As originally reported by Eddi *et al.*[1], when the pair is sufficiently close, the asymmetry in the wavefield along their line of centers causes them to propagate through a ratcheting mechanism. We report the results of a combined experimental and theoretical investigation of ratcheting pairs of bouncing droplets. Particular attention is giving to rationalizing the reversals in directions observed as the vibrational forcing is increased progressively. Our study highlights the shortcomings of the stroboscopic models of bouncing droplets in situations where the vertical bouncing dynamics are variable and droplets interact through the propagating wave fronts generated during impact.

I. INTRODUCTION

Coalescence of a millimetric droplet with an underlying bath of the same fluid can be avoided by vibrating the bath vertically[2] with acceleration $\gamma \sin \omega t$, provided the vibrational frequency, ω, is comparable to the natural oscillation frequency of the drop, $\omega_d \sim \sqrt{\sigma/\rho R^3}$, where σ, ρ and R denote, respectively, the surface tension, density and radius of the drop. As the droplet bounces on the free surface, it interacts with waves triggered by its previous impacts. For a drop of a given size, there is a critical vibrational acceleration γ_B, the bouncing threshold, below which it coalesces and above which it bounces. The bouncing mode depends on γ, and is characterized

by the ordered pair (m, n): in the (m, n) mode, the drop bounces n times in m periods of the bath oscillation. For γ just above γ_B, the drop bounces in place with the same frequency as the driving, in the $(1, 1)$ mode. As γ is further increased, the bouncing mode changes according to a sequence that depends on drop size, that may include $(2, 2)$, $(4, 4)$ or $(4, 3)$ modes[3–6]. Eventually, once the drop's bouncing amplitude is sufficiently large, it bounces at twice the frequency of the driving, in the $(2,1)$ mode. The drop then achieves resonance with the most unstable wave mode of the bath, namely the subharmonic Faraday waves excited by its impact. Consequently, this period-doubling transition is accompanied by a dramatic increase in the amplitude of the droplet's wavefield[2]. Further increasing γ beyond the walking threshold, γ_W, may serve to destabilize the resonant bouncer into a dynamic state, the so-called *walker*, in which the droplet self-propels by virtue of a resonant interaction with its own wavefield[7]. Increasing γ beyond the Faraday threshold, γ_F, prompts the emergence of a standing field of subharmonic Faraday waves throughout the bath. The Faraday wavelength, λ_F, is calculated by Kumar[8] for a viscous fluid, and for a weakly viscous fluid is well approximated by the standard water-wave dispersion relation.

Eddi *et al.*[1] demonstrated that bouncing droplet pairs of unequal size may self-propel through a ratcheting motion. Notably, this ratcheting motion arises below the walking threshold of the individual droplets, and so is due exclusively to the wave-mediated droplet interaction. They demonstrated that as γ is increased progressively, the direction of motion of the ratcheting pairs along their line of centers may reverse twice, and argued that these reversals in direction were due to changes in the vertical bouncing modes of the individual drops. Specifically, at the lowest memory at which ratcheting occurs, they found that both drops are in the $(1,1)$ mode, and the large drop follows the small. As γ was increased beyond the threshold at which the small drop period-doubles into a

---

a)C.A.Galeano.Rios@bath.ac.uk
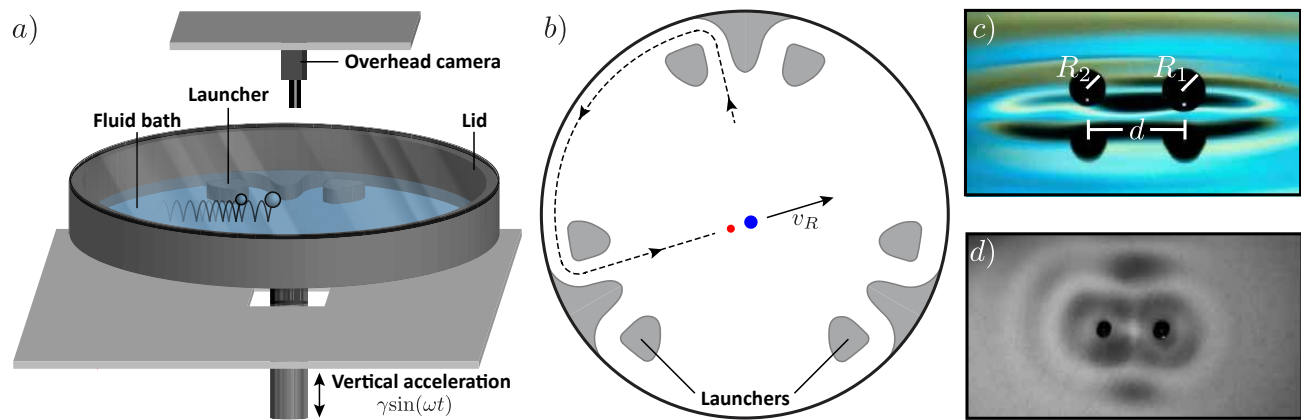b)couchman@mit.edu
c)bush@math.mit.edu

FIG. 1: a) A schematic diagram of the experimental set-up. A detailed description of the shaker can be found in Harris and Bush[9]. b) A schematic illustration showing a view of the bath as seen by the overhead camera. Submerged launchers are used to direct ratcheting pairs towards the center of the bath. c) A ratcheting pair consists of two unequally sized drops of radii R_1 and R_2 interacting at a distance d through their common wavefield. This image was captured using the visualization technique developed by Harris *et al.*[10] d) An overhead view of the wavefield generated by a ratcheting pair.

(2,2) mode, they found that the smaller drop then follows the larger one. Finally, upon further increasing γ, so that the larger drop also enters the (2,2) mode, they found that the large drop once again follows the small, but at a separation distance larger than that arising for (1,1) bouncers. By exploring a broader parameter regime, we demonstrate here that up to four reversals of direction may arise for a given droplet pair as γ is increased. Furthermore, we show that the majority of these reversals in direction are not caused by changes in bouncing mode, but rather by changes in the impact phase within a given mode, which can alter both the magnitude and direction of the net wave force exerted on the pair by the waves during impact.

The stroboscopic model of Oza, Rosales, and Bush[11] has proven to be sufficient for predicting the stability of a variety of single-walker states, including the bouncing and walking states, as well as circular orbits in a rotating frame[4,11] and in the presence of a simple harmonic potential[12,13]. However, the stroboscopic model cannot be expected to capture the behavior of ratcheting pairs for several reasons. First, the stroboscopic model does not account for variations in a drop's vertical dynamics and so would be unable to capture the range of bouncing modes, including (1,1), (2,2) and (2,1) modes, seen in our experiments. Second, the stroboscopic model is unable to capture modulations in bouncing phase, an effect shown to be important when modeling droplet-droplet interactions in orbiting[14] and promenading[15] pairs. Third, the stroboscopic model assumes implicitly that a standing field of Faraday waves is generated at each impact and that the impact between the drop and bath is instantaneous. Experimental measurements by Damiano *et al.*[16] have shown that a droplet's wavefield actually has radially propagating wavefronts. In the parameter regime examined in our experiments, the contact time

Pair	A	B	C	D	E
R_1 (mm)	0.444	0.406	0.400	0.383	0.406
R_2 (mm)	0.353	0.354	0.361	0.365	0.393

TABLE I: The radius of the larger drop, R_1, and the smaller drop, R_2, for the five ratcheting pairs considered in our experiments. The pairs are labeled in order of largest (pair A) to smallest (pair E) difference in drop size. All drop radii have an experimental uncertainty of approximately ± 0.01mm.

between the drop and the bath is sufficiently long that the horizontal dynamics of the drops is significantly influenced by the traveling wave fronts generated during impact.

To characterize the dynamics of ratcheting pairs theoretically, we adopt the model of Milewski *et al.*[5], which uses weakly viscous quasi-potential theory to more accurately capture the wavefield generated by a droplet. Notably, the wavefield predicted by this model was shown to be in good agreement with the experimental wavefield measurements of Damiano *et al.*[16]. Specifically, it captures the radially propagating wavefronts generated at each drop impact. Further, the model of Milewski *et al.*[5] is able to capture the variety of bouncing modes observed in experiment, by explicitly modeling the drop's vertical dynamics and the drop's interaction with the bath surface during contact.

In section II, we detail our experimental protocol and present the results of our experimental characterization of ratcheting pairs. In section III, we briefly recap the model being used in our accompanying theoretical study, highlight the mechanism responsible for the ratcheting motion, and compare the results of our experiments and simulations. The critical insights provided by our simu-

lations are discussed in section IV.

II. EXPERIMENTS

Experiments were performed using the set-up shown in figure 1. An electrodynamic shaker[9] is used to vertically vibrate a bath of silicon oil (density $\rho = 949$ kg m^{-3}, surface tension $\sigma = 20.6 \times 10^{-3}$ N/m, kinematic viscosity $\nu = 20$ cSt) with an acceleration of $\gamma \sin \omega t$. For this fluid, the sub-harmonic Faraday waves have a wavelength of $\lambda_F \approx 4.75$mm and the Faraday threshold is $\gamma_F \approx 4.3g$, where g denotes the gravitational acceleration. Droplets of a desired size, composed of the same fluid, are created using a piezoelectric droplet generator[17]. A ratcheting pair is formed by generating two unequal drops, of radii R_1 and R_2, and by manually pushing them together until they settle into a stable bound state with an inter-drop distance d. As reported by Eddi et $al.$[18], there are a discrete set of stable separation distances. Following the convention of Eddi et $al.$[18], we use the binding numbers $n = 1, 1.5, 2, 2.5, ...$ to denote the quantized stable binding lengths. Integer and half-integer values of n denote that the drops in a pair will bounce in- or out-of-phase, respectively, after they have undergone the period-doubling transition from a $(1,1)$ to a $(2,2)$ mode.

An overhead camera is used to record the horizontal trajectory of the droplets and a transparent lid is used to isolate the bath from ambient air currents[19]. Three submerged acrylic launchers are spaced evenly around the bath's edge and serve to direct ratcheting pairs toward the bath's center. This geometric adaptation makes data collection more efficient, allowing the experiment to run relatively continuously by eliminating the need to remove the lid in order to reposition the drops after they reach the bath's edge. Following Eddi et $al.$[1], we define the ratcheting speed, v_R, to be the speed of the pair's center of mass along the radial direction between the drops, and use the convention that $v_R > 0$ when the smaller drop follows the larger drop.

We considered droplet pairs with five different size differentials, denoted A through E in table I. For each pair, we characterized the dependence of the inter-drop distance, d, and the ratcheting speed, v_R, on the driving acceleration of the bath, γ, and the pair's binding number, n. For a given pair size, the driving acceleration of the bath was first set to $\gamma = 1.2g$, slightly above the bouncing threshold, γ_B, and an initial separation distance corresponding to binding number $n = 1, 1.5, 2$ or 2.5 was chosen. Note that at $\gamma = 1.2g$, all drops bounce in phase in a $(1,1)$ mode: the possibility of the drops being out of phase only arises when both drops are above the period-doubling transition. No ratcheting motion was observed for pairs with binding numbers $n > 2.5$: the wave force imparted during impact at such large separation distances is evidently too weak to generate horizontal motion and the droplets bounce in place. For a given pair size and binding number, n, γ is then slowly

increased in increments of $0.1g - 0.2g$. As γ is increased progressively, the pair first transitions from a static to a ratcheting state, and then the ratcheting state eventually destabilizes into an orbiting state. At each increment of γ, an overhead video of the pair is recorded at a frame rate of 5 fps, allowing us to track the horizontal motion of each drop. We note that for pair A, which has the largest size differential, ratcheting motion with binding number $n = 1$ was observed all the way down to the value of γ at which the larger drop coalesced with the bath. A video showing several examples of the ratcheting motion of pair A with binding number $n = 1$ is included in the supplementary materials.

Figure 2 shows the dependence of the inter-drop distance, d, on the dimensionless driving acceleration, γ/γ_F, for ratcheting pairs A through E for each accessible binding number n. We note that pair E, which has the smallest size differential, exhibited no ratcheting motion beyond a binding number of $n = 1.5$, and pair A, which has the largest size differential, was the only pair to exhibit ratcheting motion at $n = 2.5$. Figure 2 suggests that the shift in d with increasing γ may be attributed to the shift in the wavelength of a drop's wavefield as the drop transitions through various bouncing modes to reach the $(2,1)$ mode. We observe that this shift is most pronounced for pairs with binding number $n = 1$. Note that below the period-doubling transition, all drops bounce in phase, while above it, the drops bounce either in phase or out of phase according to their separation distance.

Figure 3 shows the dependence of the ratcheting speed, v_R, on γ/γ_F for pairs A through E for each accessible binding number n. The largest ratcheting speeds are seen to occur when the drops are closest together and when the size difference between the drops is largest. Multiple reversals in direction are apparent as γ is increased. The number of reversals and the values of γ/γ_F at which they occur are weakly dependent on the pair's size and strongly dependent on the binding number n.

III. MODELING

We simulate the behavior of ratcheting pairs using the theoretical model developed by Milewski et $al.$[5]. This model relies on a linear quasi-potential approximation of the free surface flow[20], in which the effects of impacting droplets are included by means of a time-dependent moving pressure field. The free surface elevation, η, and the velocity potential, $\phi(x, y, z, t)$, of the fluid bath are governed by the equations

$$0 = \Delta\phi, \tag{1}$$

$$\phi_t = -g(1 + \gamma \sin(\omega t))\eta + \frac{\sigma}{\rho}\Delta_H\eta + 2\nu^*\Delta_H\phi - \frac{P}{\rho}, \tag{2}$$

$$\eta_t = 2\nu^*\Delta_H\eta + \phi_z, \tag{3}$$

where $\Delta = \partial_{xx} + \partial_{yy} + \partial_{zz}$, $\Delta_H = \partial_{xx} + \partial_{yy}$, $P = P(x, y, t)$ is the forcing term that models the effect of
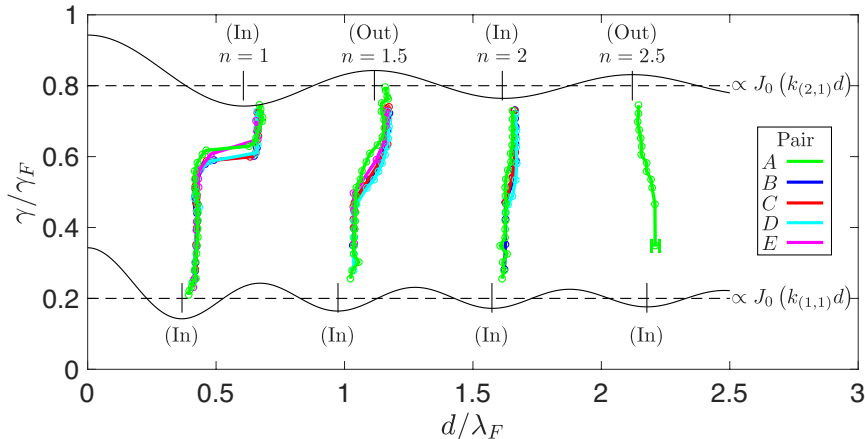
FIG. 2: The dependence of the dimensionless inter-drop distance, d/λ_F, on the dimensionless driving acceleration of the bath, γ/γ_F, for ratcheting pairs of size A through E and binding numbers $n = 1$ to $n = 2.5$. In each dataset, the bottommost point corresponds to the value of γ/γ_F at which the pair first starts ratcheting (or below which coalescence occurs for pair A, $n = 1$) and the topmost point indicates when the ratcheting pair destabilizes into an orbiting pair. The experimental uncertainty on d is approximately ± 0.1mm, as determined by the resolution of the overhead camera. Smooth curves have been drawn through the data for the sake of clarity and the corresponding ratcheting speeds are shown in figure 3. The relative vertical bouncing phase of the drops for each pair (in or out of phase) at the beginning and end of the ratcheting regime is indicated. For the sake of comparison, Bessel functions $J_0\left(k_{(1,1)}d\right)$ and $J_0\left(k_{(2,1)}d\right)$ are shown, which are the wave fields produced respectively by $(1,1)$ and $(2,1)$ bouncers, located at $d = 0$; as predicted by the stroboscopic model[11]. Note that $k_{(1,1)} = 2.20$mm^{-1} and $k_{(2,1)} = 1.32$mm^{-1} are the wavenumbers obtained from the water-wave dispersion relation using forcing frequencies of 80Hz and 40Hz, respectively.

the impacting droplets, and the constants σ, ρ and g denote, respectively, the surface tension, liquid density and gravitational acceleration. Equation (1) is valid in the semi-space $z < 0$, and equations (2) and (3) in the xy-plane.

The constant ν^* is the corrected value of the kinematic viscosity, ν, required to match the Faraday threshold, γ_F, observed in experiments[5]. For the experimental parameters used here, the effective viscosity $\nu^* = 0.8025\nu$. The equations of the model are formulated in the frame of reference of the shaker, which requires the use of a time dependent gravity field, $G(t) = g\left(1 + \gamma \sin \omega t\right)$. A thorough derivation of these equations is presented in Galeano-Rios, Milewski, and Vanden-Broeck[6]. Periodic boundary conditions are imposed in x and y, allowing the use of spectral methods. Spectral decomposition also diagonalizes the Dirichlet-to-Neumann map, defined as $\phi(x, y, 0, t) \mapsto \phi_z(x, y, 0, t)$, which is necessary to reduce equations (2) and (3) to a two-dimensional problem in the plane $z = 0$.

In flight, a droplet's motion is described by

$$\frac{d^2 z_i}{dt^2} = -G(t), \qquad (4)$$

$$m_i \frac{d^2 \mathbf{x}_i}{dt^2} = -6\pi R_i \mu_{air} \frac{d\mathbf{x}_i}{dt}, \qquad (5)$$

where $\mathbf{x}_i = (x_i, y_i)$, (x_i, y_i, z_i) are the coordinates of the lowermost point ('south pole') of the i-th droplet and R_i, m_i and μ_{air} denote, respectively, the radius and mass of the i-th droplet and the dynamic viscosity of air. While air drag is significant in the drop's horizontal motion, it is negligible in its vertical motion[21].

A droplet's impact is defined as the period of time during which the south pole of the droplet is predicted to be below the level of the free surface, the latter being calculated without the forcing due to the ongoing impact pressure. During impact, the vertical motion of a droplet is calculated using the non-linear spring model of Moláček and Bush[3], namely,

$$\left(1 + \frac{c_3}{\ln^2\left|\frac{c_1 R_i}{z_i - \bar{\eta}_i}\right|}\right) m_i \frac{d^2 z_i}{dt^2} + \frac{4\pi \nu \rho R_i c_2}{3\ln^2\left|\frac{c_1 R_i}{z_i - \bar{\eta}_i}\right|} \frac{d}{dt}(z_i - \bar{\eta}_i) + \frac{2\pi\sigma}{\ln\left|\frac{c_1 R_i}{z_i - \bar{\eta}_i}\right|}(z_i - \bar{\eta}_i) = -m_i G(t), \qquad (6)$$

where the values of the constants c_1, c_2 and c_3 are as

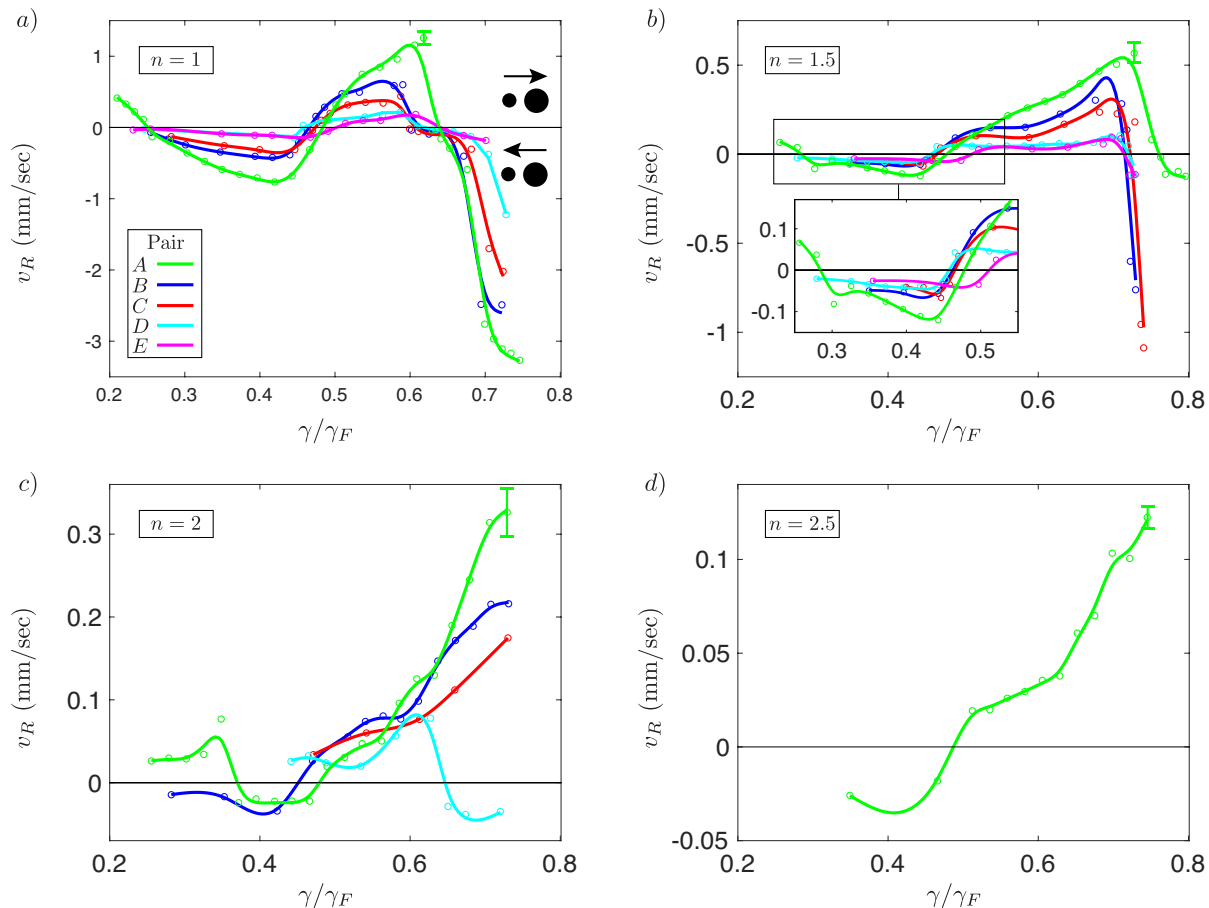given in Milewski et al.[5]. The variable $\bar{\eta}_i$ is the estimate

FIG. 3: The dependence of the ratcheting speed, v_R, on the dimensionless driving acceleration of the bath, γ/γ_F, for ratcheting pairs of size A through E and binding numbers a) $n = 1$, b) $n = 1.5$, c) $n = 2$, and d) $n = 2.5$. We use the convention that v_R is positive when the smaller drop follows the larger drop. Each reported v_R is obtained by averaging the ratcheting speeds measured in two separate trials and the associated experimental uncertainty is approximately $\pm 10\%$. For each curve, the leftmost point corresponds to the value of γ/γ_F at which the pair first starts ratcheting (or below which coalescence occurs for pair A, $n = 1$) and the rightmost point indicates when the ratcheting pair destabilizes into an orbiting pair. Smooth curves are drawn through the data for the sake of clarity.

of the free surface elevation at $\mathbf{x}_i$, as would arise in the absence of the drop impact in question. It is calculated from a separate solution of the free surface flow, that is not subject to the forcing of the current impact of the i-th droplet. The variable $\bar{\eta}_i$ is required if a spring model is used to account for the interaction between the droplet and the bath, as $(z_i - \bar{\eta}_i)$ prescribes the intrusion depth of the impacting droplet. Since we here have two droplets to consider, at times we need to calculate up to three free surfaces; namely, that resulting from the impact of both droplets, and those arising from the individual impacts. The vertical force that the bath exerts on the i-th droplet is given by $F_i(t) = \max\left(0, m_i(d^2 z_i/dt^2) + m_i G(t)\right)$. We note that suction forces, as may be significant during droplet rebound[21], are not considered. The forces $F_i(t)$ are used to calculate the pressure field

$$P(x, y, t) = \sum_i P_i(x, y, t) \qquad (7)$$

in equation (2), where

$$P_i = \frac{F_i(t)}{\pi r_i^2(t)} \chi(\{(x, y), |(x, y) - (x_i, y_i)| < r_i(t)\}), \quad (8)$$

with $r_i(t) = \min(\sqrt{2|z_i - \bar{\eta}_i| R_i}, R_i/3)$, and χ is the characteristic function of the pressed area. These modeling choices are made following those of Milewski et al.[5]

The horizontal motion of the droplet during impact is determined by

$$m_i \frac{d^2 \mathbf{x}_i}{dt^2} + D(t) \frac{d\mathbf{x}_i}{dt} = -F_i(t) \nabla \bar{\eta}_i|_{\mathbf{x}_i}, \qquad (9)$$

$$D(t) = c_4 \sqrt{\frac{\rho R_i}{\sigma}} F(t) + 6\pi R_i \mu_{air}, \qquad (10)$$

as was developed by Moláček and Bush[3]. We use a value of $c_4 = 0.13$ for the horizontal drag coefficient[5]. We note that equation (5), used during flight, is simply equation (10) for the case $F(t) = 0$.
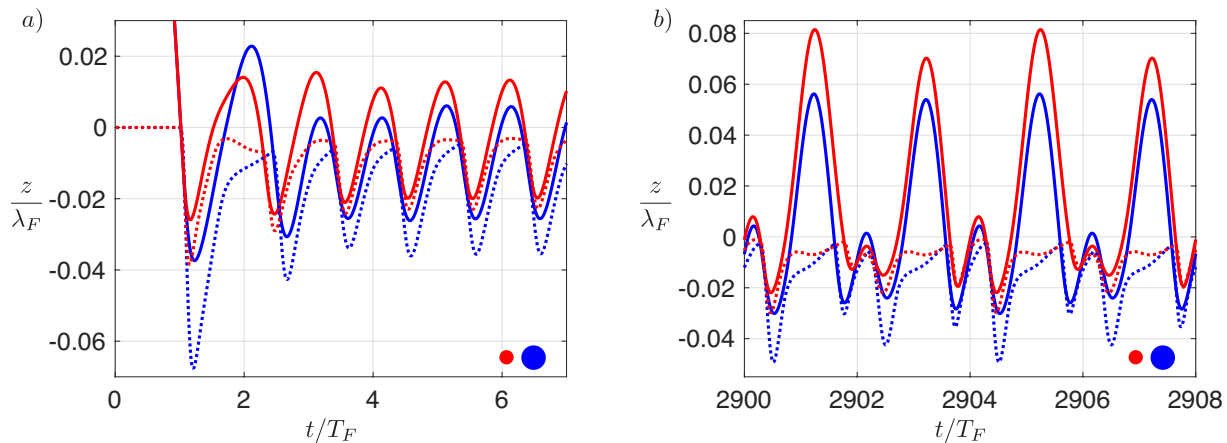
FIG. 4: Examples of the simulated vertical motion of droplets in ratcheting pair A with binding number $n = 1$. The solid blue and red lines denote the heights of the south poles of the larger and smaller drops, respectively. The dashed blue and red lines show the heights of the free surface beneath each drop. Panel a) shows the initial transient at the start of the simulation as the droplets settle into $(1, 1)$ bouncing modes at $\gamma/\gamma_F = 0.2$. Panel b) shows both droplets bouncing in a $(2, 2)$ mode at $\gamma/\gamma_F = 0.62$.
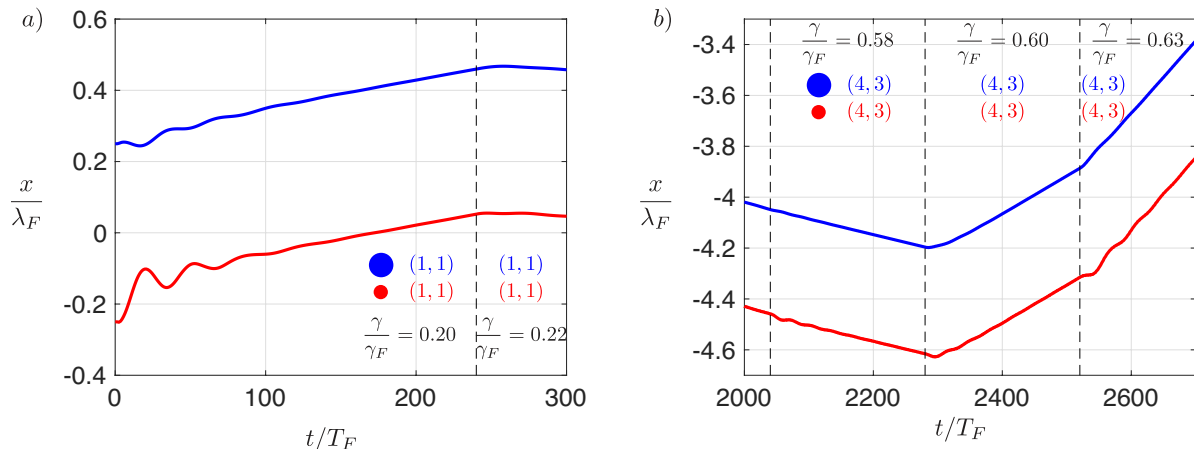

FIG. 5: Examples of the simulated horizontal motion of droplets in ratcheting pair A with binding number $n = 1$. The blue and red lines indicate the horizontal positions of the larger and smaller droplets respectively. The dashed vertical lines indicate the times at which the driving acceleration was increased by $\gamma = 0.1g$. Panel a) shows the initial transient at the start of a simulation as the pair settles into the stable binding length corresponding to $n = 1$. In this panel, we can also see the first reversal taking place at $\gamma/\gamma_F = 0.22$, beyond which the droplets start to move at an extremely slow speed in the opposite direction. Panel b) shows examples of how the ratcheting speed changes with successive increments in γ.

A. Simulations

We chose to focus our simulations on pairs A and B with binding numbers $n = 1, 1.5$ and 2, as these pairs exhibited the richest behavior in our experiments. Each simulation is initialized by releasing a pair of droplets, separated by a distance d, from a height of 1mm onto an undisturbed fluid surface at time $t = 0$, with $\gamma/\gamma_F = 0.2$. The initial inter-drop distance, d, is varied to obtain pairs of different binding numbers, n. After an initial transient, the droplets quickly settle into the $(1, 1)$ bouncing mode

and bounce with similar impact phases (figure 4a). As shown in figure 4, our simulations allow us to track the vertical trajectory of the south pole of each drop, $z_i(t)$, and the positions of the fluid interface below each drop, $\eta_i(t)$. We note that with our model, there can be a slight mismatch between z_i and η_i when the drop is in contact with the bath, owing to our method for approximating the waveform[5].

After the initial transient, the droplets begin to move horizontally as a ratcheting pair, with the smaller droplet following the larger one (figure 5a). We define the x-
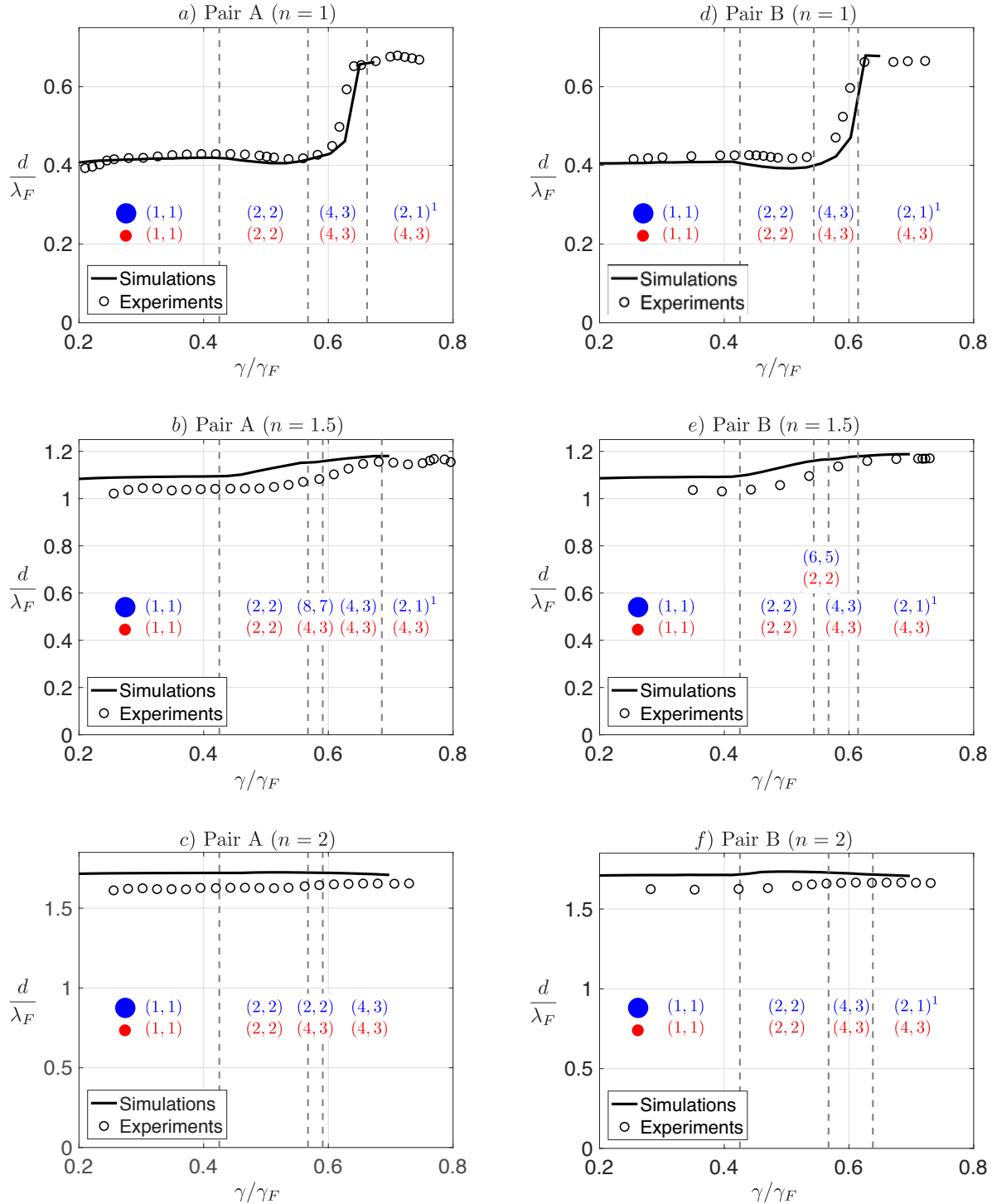
FIG. 6: A comparison of the experimental (circles) and theoretical (solid curves) dependence of the dimensionless separation distance, d/λ_F, on the dimensionless driving acceleration of the bath, γ/γ_F, for ratcheting pairs A and B in modes $n = 1$, $n = 1.5$ and $n = 2$. Vertical dashed lines indicate the changes in bouncing modes apparent in the simulations. The bouncing modes of the larger and smaller drops in the simulation are indicated in blue and red, respectively.
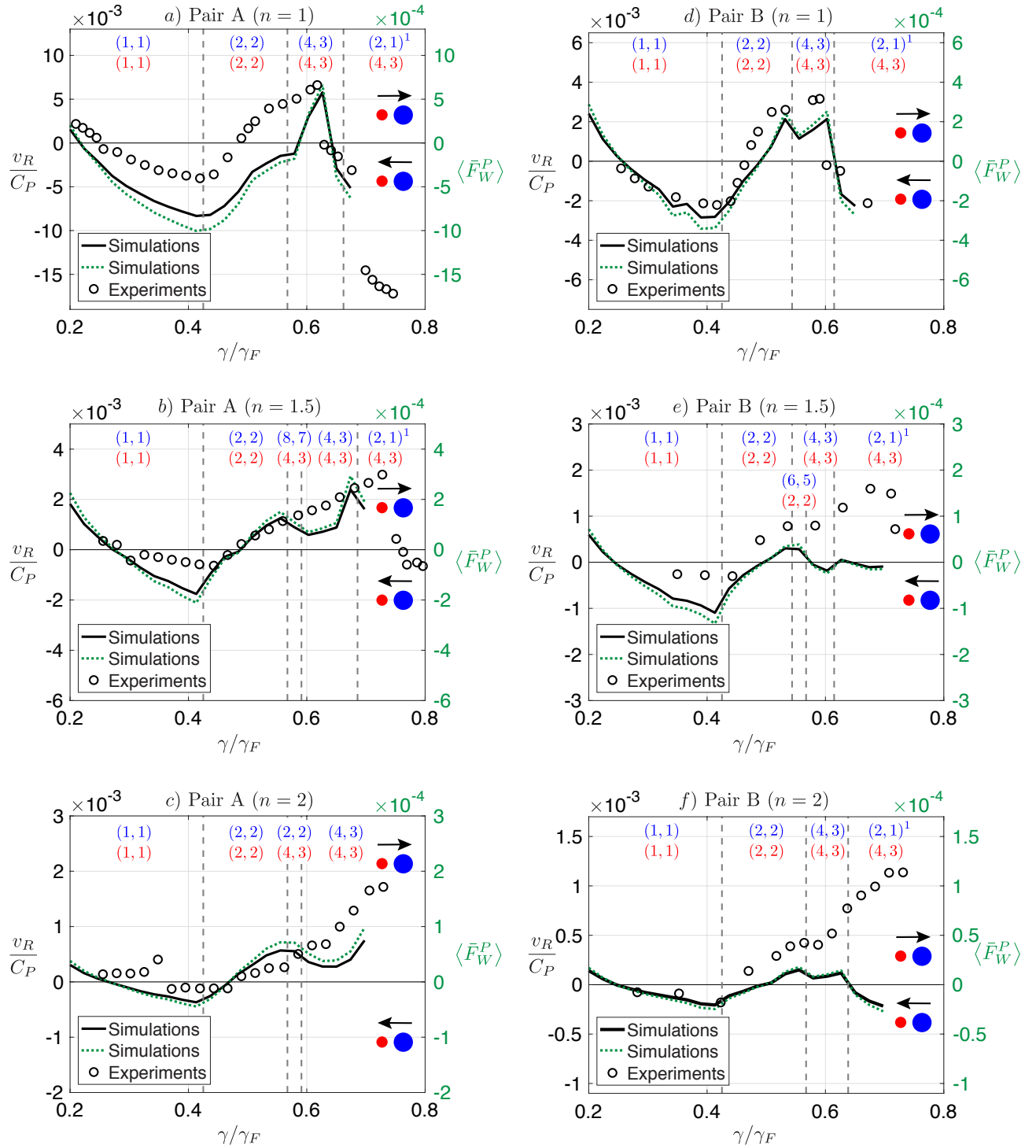
FIG. 7: A comparison of the experimental (circles) and theoretical (solid curves) dependence of the dimensionless ratcheting speed, v_R/C_P, on the dimensionless driving acceleration of the bath, γ/γ_F, for ratcheting pairs A and B in modes $n = 1$, $n = 1.5$ and $n = 2$. C_P is the phase speed of a wave with the Faraday wavelength, defined as $C_P = \lambda_F f_F$, where λ_F and f_F are the Faraday wavelength and frequency, respectively. Specifically, $C_P = 190$ mm/s in our experiments and $C_P = 188$ mm/s in our simulations. Vertical dashed lines indicate the changes in bouncing modes apparent in the simulations. The bouncing modes of the larger and smaller drops in the simulation are indicated in blue and red, respectively. The dashed green curves indicate the dimensionless, net horizontal wave force acting on the pair averaged over one bouncing period, $\langle \bar{F}_W^P \rangle = \langle F_{W,1}/m_1 g + F_{W,2}/m_2 g \rangle /2$, as calculated from our simulations.

coordinate to be along the ratcheting direction, oriented to point from the smaller drop to the larger drop. Each simulation is run at a fixed driving acceleration, γ, until the horizontal speed of both droplets, averaged over a bouncing period of the pair, converges to a steady value, at which point the ratcheting speed, v_R, is recorded. We then progressively increase γ in increments of $0.1g$, as was done in the experiments. After each increment, the pair is allowed to settle into its new equilibrium state. With each increase in γ, we observe a corresponding change in impact phase of the droplets, which affects both the accompanying wavefields generated at impact and the ratcheting speed, v_R. Figure 5 gives examples of v_R changing with specific increments of γ. Eventually, a value of γ is reached at which the drops begin to execute long-period oscillations along their line of centers, and the simulation is stopped. In certain cases, an overall motion along the line of the centers persists accompanied by a periodic oscillation of the separation distance. This behavior was not apparent in the experiments.

Figure 6 shows the dependence of the inter-drop separation distance, d, on the driving acceleration, γ, for the pairs considered in our simulations, compared directly to the experimental data. Our simulations are able to capture adequately the experimentally observed shifts in d as γ is increased, including the sharp jump observed at binding number $n = 1$. For pair B, this sharp jump in d is due to the droplets in the pair changing bouncing mode: the larger and smaller drops undergo $(4,4) \to (2,1)^1$ and $(4,4) \to (4,3)$ transitions, respectively. For pair A, the cause is more subtle as the jump in d occurs due to a change in the vertical dynamics of both drops within the $(4,3)$ mode. Specifically, the jump occurs when the drops change from taking one long bounce (of duration $2T_F$) and two short bounces (each of duration T_F) in synchrony, to the large/small drop taking the long bounce while the small/large drop takes two short bounces.

As seen in figure 6, for binding numbers $n = 1.5$ and $n = 2$, the model consistently yields a slight overprediction for the inter-drop distance, d, likely due to small errors introduced by our modeling of the waves. Specifically, the decay rate of the waves is prescribed by the effective viscosity ν^*, as was chosen to match the Faraday threshold. The model is thus unlikely to predict correctly the decay rate for driving accelerations far from the Faraday threshold. We expect the resulting error to increase with n, as the wave fronts produced by the drops take longer to arrive at their companions, so the effects of the anomalous decay rate will be more pronounced. Both trends are apparent in figure 6.

Figure 7 shows the predicted dependence of the ratcheting speed, v_R, on the driving acceleration γ, compared directly to our experimental data. The net horizontal wave force acting on the pair, averaged over a period of the pair's vertical motion, determines the direction of the ratcheting motion and is shown in green for reference. We note that the sharp jumps in separation distances observed in figures 6a and 6d correspond to sharp corners

in the velocity curve in figure 7. The corner evident at $\gamma/\gamma_F \approx 0.66$ in figure 7b, is also due to a rearrangement of the two $(4,3)$ modes of the two droplets. While similar to that described for pair A at $n = 1$, in this case it is for a pair that is out of phase.

In the majority of cases, our simulations were able to capture all of the observed reversals in ratcheting direction and the qualitative agreement between the experimental and theoretical ratcheting speeds is satisfactory. However, there are some notable discrepancies apparent for pair B at large values of γ/γ_F, where the simulations predict a reversal in ratcheting direction that was not observed in the experiments. We shall attempt to rationalize these discrepancies in what follows.

B. Details of the ratcheting mechanism

Eddi *et al.*[1] attributed the two reversals in ratcheting direction apparent in their experiments to the successive transition of the small and large drop from a $(1,1)$ to a $(2,2)$ bouncing mode. However, in our simulations, this period-doubling transition always occurs simultaneously for both droplets and is not associated with any reversal in ratcheting direction. We also note that if the drops were both emitting standing waves, one would expect the ratcheting pairs to align themselves in the extrema of the Bessel waveforms generated by their partner. Figure 2 makes clear that while such is a fair approximation, it is not precisely correct. In order to better understand what determines the inter-drop spacing, speed and direction of a ratcheting pair, we proceed by examining the coupling of each droplet with the bath.

Figure 8a shows the time-dependence of the horizontal component of the wave-force, $F_W = -F_i(t) \nabla \left. \bar{\eta}_i \right|_{\mathbf{x}_i}$, acting on each droplet in pair A with binding number $n = 1$ at $\gamma/\gamma_F = 0.2$, over a bouncing period. Figure 8a shows that the wave force acting on each drop is approximately sinusoidal, and reverses sign approximately halfway through the time of impact of the drop. The origin of this reversal in the wave force is shown in figures 8b-f. Upon impact, the wavefield produced by the previous impacts causes both drops to be attracted to each other. During impact, each droplet triggers a traveling front that propagates outward. As this front approaches the partner drop, it reverses the surface gradient, thus repelling the partner drop. If the net wave force on the pair averaged over a bouncing period, $\langle F_W^P \rangle$, is non-zero, then the pair will ratchet. The ratcheting speed is determined by the balance between the averaged net wave force and the drag force, and is equal to the speeds of the individual droplets averaged over a bouncing period. The ratcheting speed, $\sim 1 \text{mm/sec}$, is much slower than the typical walking speed of an individual drop, $\sim 10 \text{mm/sec}$, due to the small net wave force resulting from the reversal in surface gradient during contact. We note that although in our experiments the droplets look to move at a steady speed with a fixed inter-drop distance, our simulations
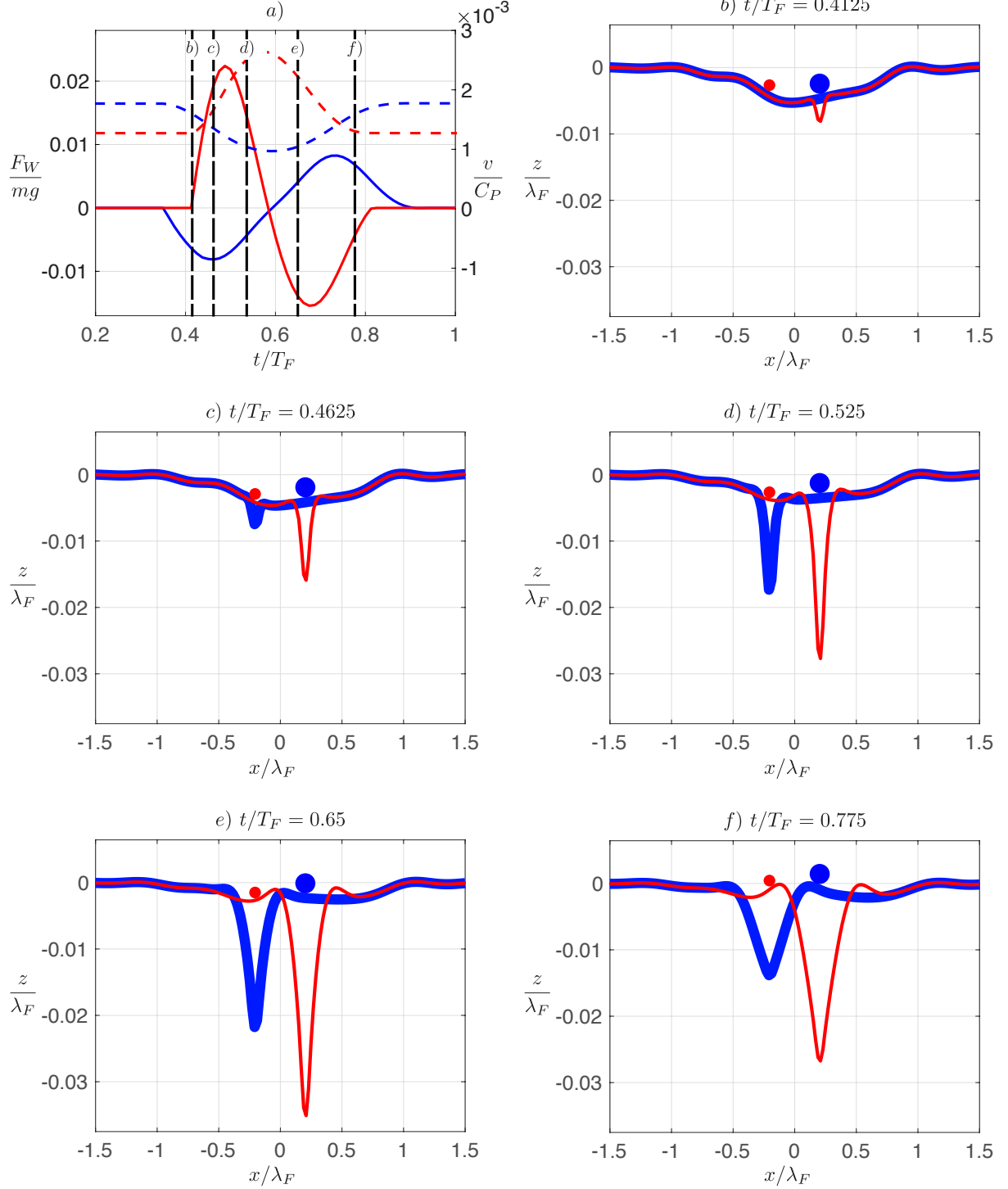
FIG. 8: a) Time dependence of the horizontal wave force, F_W, acting on each drop (solid lines) and the speed, v, of each drop (dashed lines) in ratcheting pair A with a binding number of $n = 1$ at $\gamma/\gamma_F = 0.2$. b)-f) Snapshots of the wave field at the times marked in panel a). The larger drop, and its corresponding average surface deflection $\bar{\eta}_1$ are shown in blue, the corresponding curves for the smaller droplet in red. In panel b), the impact of the larger droplet triggers the traveling front that moves toward the smaller droplet. In c), the smaller droplet impacts, triggering the second moving front. In d), the horizontal force is still inward for both droplets as the fronts have not yet moved enough to reverse the surface gradient. In e), the surface gradient is reversed by the traveling fronts. In f), the fronts continue to move past the droplets, reversing the forces until the end of contact.
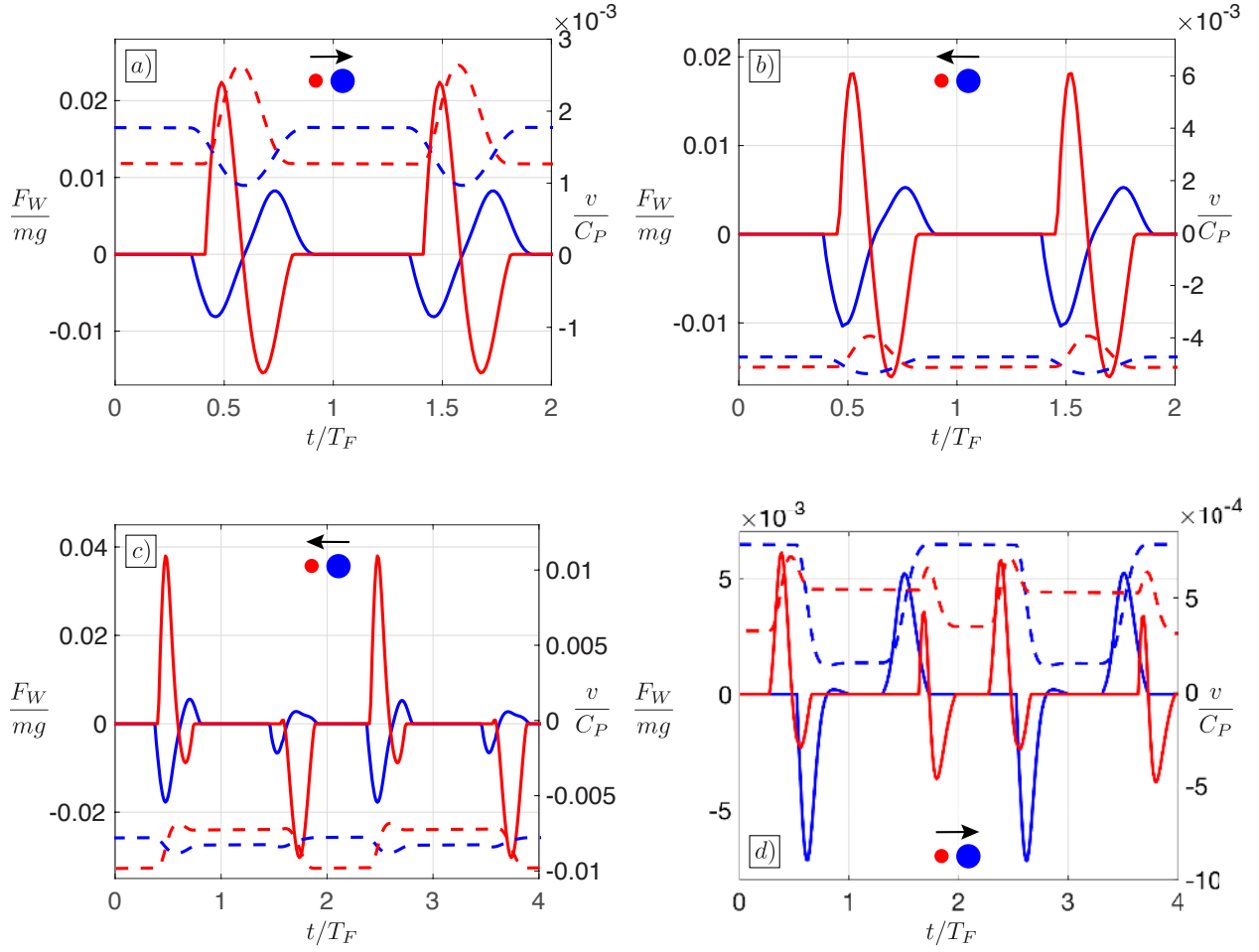
FIG. 9: The time dependence of the horizontal wave force, F_W, acting on each drop (solid lines) and the speed, v, of each drop (dashed lines) for pair A with binding number n and driving acceleration γ/γ_F as follows: a) $n = 1, \gamma/\gamma_F = 0.2$, b) $n = 1, \gamma/\gamma_F = 0.25$, c) $n = 1, \gamma/\gamma_F = 0.44$, d) $n = 1.5, \gamma/\gamma_F = 0.51$. In panels a) and b) both drops are in $(1, 1)$ bouncing modes. In panels c) and d) both drops are in $(2, 2)$ bouncing modes.

have highlighted that the speed of each droplet is actually fluctuating over the timescale of contact with the bath (figure 8a).

The reversal of the horizontal wave force on each droplet was observed for all of the ratcheting pairs considered in our simulations, some examples of which are shown in figure 9. These reversals in wave force are expected when the time between successive wave crests at a given point is comparable to a droplet's contact time. Whether the wave force averages to a positive or negative value is highly sensitive to the phase of impact of each droplet with the bath and explains why many reversals in direction occurred *within* a given bouncing mode. For example, figure 9a) shows the wave force acting on pair A in the $(1, 1)$ bouncing mode with a binding number of $n = 1$ at $\gamma/\gamma_F = 0.2$. In this case, the wave forces on each drop average to a positive value and the small drop follows the large. However, as shown in figure 9b), if the driving acceleration is increased to $\gamma/\gamma_F = 0.25$, although the drops remain in a $(1, 1)$ bouncing mode,

the phase of impact has changed sufficiently that the net wave forces imparted to each drop assume negative values, so the large drop follows the small. We note that changes in bouncing mode that result in sharp differences in bouncing phase (e.g. the $(4, 3) \rightarrow (2, 1)^1$ transition) cause sudden variations in the ratcheting velocity. All instances in which the velocity curves in figure 7 have a discontinuity in slope arise in the vicinity of discrete changes in bouncing mode.

The reversal of the wave force during impact also allows us to rationalize why ratcheting pairs have a discrete set of inter-drop distances. As shown in figure 10, a series of moving wave fronts travel away from the location of each droplet impact. In order to be horizontally stable, the drops in a pair must be separated by a distance such that, during the impact of each drop, a minimum in the traveling wave front emitted by its partner sweeps beneath it, causing a reversal in the wave force. For example, figures 10a and c show that for binding numbers $n = 1$ and $n = 2$, the larger (blue) droplet in pair A
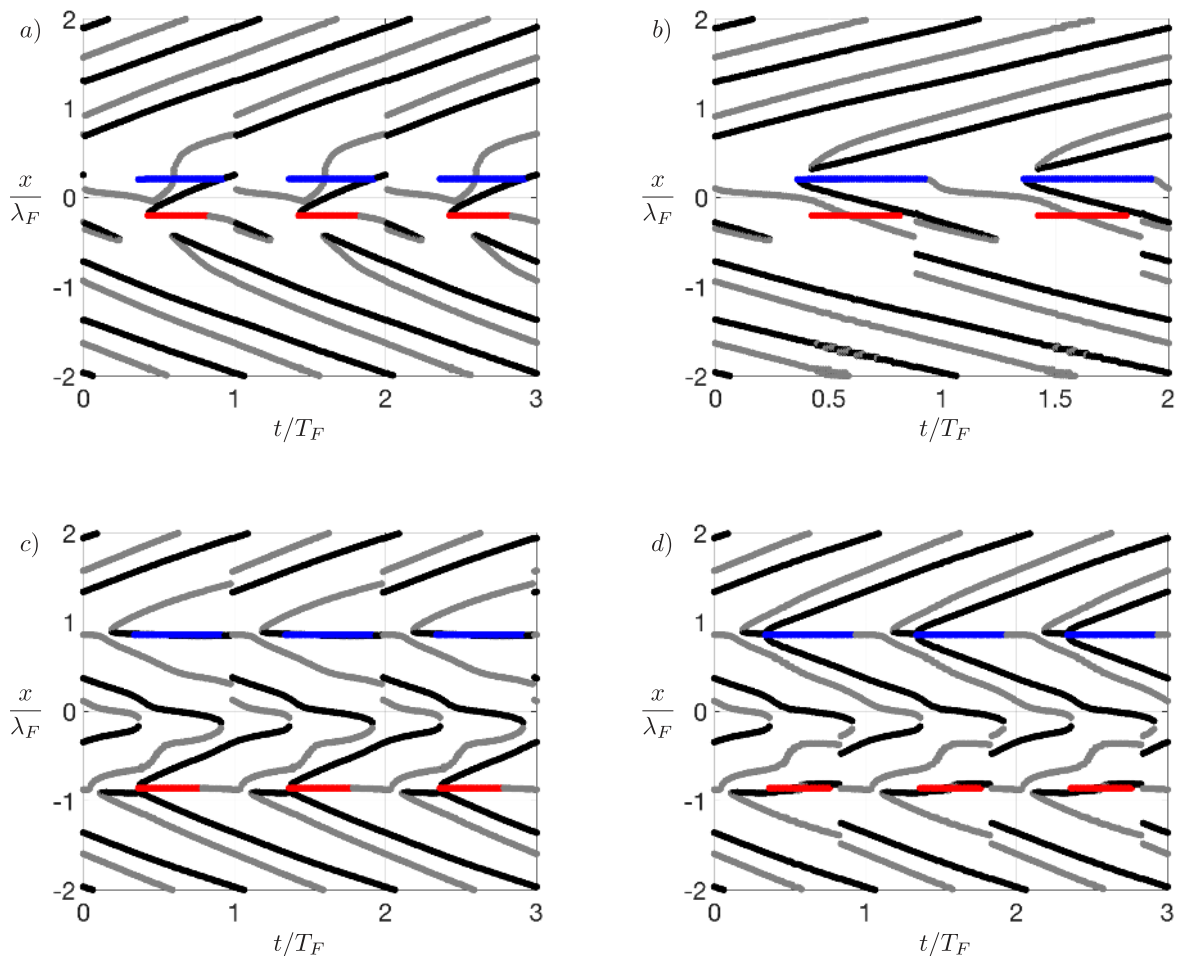
FIG. 10: The positions of droplet impact in relation to the moving extrema of the wavefield for ratcheting pair A at $\gamma/\gamma_F = 0.2$. Maxima and minima of the wavefield are indicated in black and gray, respectively, and the impact positions of the smaller and larger droplets are denoted by red and blue, respectively. Panels a) and b) show the extrema of $\bar{\eta}_1$ and $\bar{\eta}_2$, respectively, for $n = 1$ and panels c) and d) show the extrema of $\bar{\eta}_1$ and $\bar{\eta}_2$, respectively, for $n = 2$.

always impacts at a position such that a minimum produced by the smaller (red) droplet sweeps beneath it during contact. Similarly, figures 10b and d show that the minimum produced by the larger (blue) droplet sweeps beneath the smaller (red) droplet during impact. Figure 10 also highlights that an accurate picture of the wave field must include traveling fronts, consideration of which are necessary to rationalize the changes in surface slope that take place during impact.

In order to understand why the quantized inter-drop distances are stable, consider the standing Bessel wavefields shown in figure 2, which represent a snapshot, at the time of impact, of the moving fronts. Due to the finite contact time of each drop with the bath, each drop must first impact slightly to the right of a minimum produced by the partner drop, so that the inter-drop distance initially starts to decrease. The minimum then sweeps outward beneath the drop, causing the surface gradient to

reverse and the inter-drop distance to increase again, resulting in a net change in the inter-drop distance of zero. This is a stable position because if the inter-drop distance d is slightly larger than the stable position, the traveling fronts take longer to arrive and so they reverse the surface gradient at a later stage of the contact, leading to a net attraction. Similarly, if d is decreased, the traveling fronts arrive earlier, causing a net repulsion. One may thus rationalize why the standing wave-model (see figure 2) always slightly underestimates the stable separation distances; specifically, it neglects the interaction of the drops with the traveling wave fronts during their finite contact time.

Finally, we address the discrepancies previously mentioned between our experimental and theoretical results. In figure 7, the simulated velocity curves sometimes have kinks that are not present in the experimental data (such as between $\gamma/\gamma_F \approx 0.6 - 0.7$ in figure 7b). For pair B,

with binding numbers of $n = 1.5$ and $n = 2$ (figures 7e and f, respectively), the simulations also predict an additional reversal in direction that was not observed in our experiments. The most likely cause for these discrepancies is differences in the simulated and experimental bouncing modes. Although the wave-model of Milewski *et al.*[5] has been verified against experimental data[16], coupling it to the logarithmic spring model can result in spurious bouncing modes not seen in experiment[5]. As the ratcheting motion is highly sensitive to the bouncing phase of the droplets, if the model predicts a different bouncing mode than that seen in experiment, we should expect spurious results. For example, in figure 7b, if pair A in the $n = 1.5$ mode smoothly transitioned from a $(2, 2)$ to a $(2, 1)$ mode instead of passing through the $(8, 7)$ and $(4, 3)$ modes deduced from the simulations, the erroneous abrupt changes in the ratcheting speed not seen in experiments might have been averted. We note that the shortcomings of the current simulations might be eliminated through application of the most recent model of Galeano-Rios, Milewski, and Vanden-Broeck[6], which more accurately models the droplet-bath interaction and has been shown to predict bouncing modes more accurately.

IV. DISCUSSION

We have reported the results of an experimental study of ratcheting pairs. Five distinct pairs were considered, in up to four binding lengths, and their behavior characterized as γ was increased progressively. Eddi *et al.*[1] observed that the inter-drop distance was quantized, owing to dynamic constraints imposed on the droplets by their shared wavefield, and observed up to two reversals in ratcheting direction. We extended the work of Eddi *et al.*[1], to characterize how the stable inter-drop distances shift with increasing γ and demonstrated that up to four reversals in direction could occur for pairs with a sufficiently large drop size differential and a binding number of $n = 1$. The majority of these reversals were not correlated with a bouncing mode transition of a single droplet[4,21,22], as suggested by Eddi *et al.*[1], prompting a detailed theoretical investigation of the mechanism through which the droplets interact.

To understand the complex, wave-mediated coupling between the two droplets in a ratcheting pair, we adopted the theoretical model of Milewski *et al.*[5], wherein both the droplet's vertical dynamics and the traveling wave fronts produced by a droplet impact are modeled explicitly. Our simulations were able to closely reproduce the shift in the stable inter-drop distances with increasing γ, and provided adequate agreement with the experimentally observed ratcheting speeds. Importantly, the simulations provided critical insight into the mechanism governing the ratcheting dynamics. At every impact, each droplet produces a Bessel shaped wavefield whose extrema travel radially outwards. The partner drop then interacts with one of these traveling fronts during impact. In order to remain in a stable position, the droplet must bounce in a position such that as a traveling front sweeps past during impact, the gradient of the wavefield beneath the drop reverses direction so that the net wave force on the droplet during contact is zero. This explains why all of the experimentally observed inter-drop distances lie slightly to the right of an extremum anticipated on the basis of a standing wave model (figure 2). The drop must first land slightly to the right of an extremum in the wavefield produced by the partner drop so that it first encounters an attractive wave force. Then, as the extremum sweeps by the drop during contact, the wave force becomes repulsive, resulting in a net wave force of zero.

If the droplet lands slightly earlier or later than the critical impact time that results in a zero net force, it will cause ratcheting motion. The ratcheting speed is much slower than that of an individual walker because the reversal in the wave force during the contact time leads to a small net force. Our study also rationalizes how a reversal in direction can occur within a given bouncing mode. For example, figure 8a) shows the time evolution of the wave force during contact on pair A with a binding number $n = 1$ at $\gamma/\gamma_F = 0.2$. In this case, the net wave force on both drops is positive and the small drop follows the larger. As γ is increased, however, the bouncing phase of the droplets slowly change, the net force changes from positive to negative, and the ratcheting pair reverses direction.

We note that while the stroboscopic model[11] accurately captures the shape of the wavefield at an instant in time[16], it does not capture the outward radial expansion of the fronts. Therefore, the stroboscopic model should be used with caution when the contact time between the drop and the bath is sufficiently large that the wave force during contact changes appreciably, as is the case in our study. One can now better understand the shortcomings of the stroboscopic models[3,11,23] in rationalizing the observed behavior of orbiting[14] and promenading[15] pairs. For example, the inclusion of traveling wave fronts could account for the stability of orbiting pairs with binding number $n = 0.5$ which have been shown to be stable in experiment but cannot be captured with the stroboscopic model[14]. The neglect of the traveling fronts in the stroboscopic models also suggests their limitations in rationalizing the relative stability of various dynamical states through consideration of the system's global energetics. For example, in order for the binding energy of promenading pairs[15,24] to be a meaningful system diagnostic, it must capture the influence of the moving wave fronts.

V. SUPPLEMENTARY MATERIAL

A supplementary video is included that shows four examples of the ratcheting motion of pair A with binding

number $n = 1$.

VI. ACKNOWLEDGMENTS

[1] A. Eddi, D. Terwagne, E. Fort, and Y. Couder, "Wave propelled ratchets and drifting rafts," Europhys. Lett. **82** (2008).

[2] Y. Couder, E. Fort, C. H. Gautier, and A. Boudaoud, "From bouncing to floating: Noncoalescence of drops on a fluid bath," Phys. Rev. Lett. **94** (2005).

[3] J. Moláček and J. W. M. Bush, "Drops walking on a vibrating bath: towards a hydrodynamic pilot-wave theory," J. Fluid Mech. **727**, 612–647 (2013).

[4] O. Wind-Willansen, J. Moláček, D. M. Harris, and J. W. M. Bush, "Exotic states of bouncing and walking droplets," Phys. Fluids **25** (2013).

[5] P. Milewski, C. A. Galeano-Rios, A. Nachbin, and J. W. M. Bush, "Faraday pilot-wave dynamics: modeling and computation," J. Fluid Mech. **778**, 361–388 (2015).

[6] C. A. Galeano-Rios, P. A. Milewski, and J.-M. Vanden-Broeck, "Non-wetting impact of a sphere onto a bath and its application to bouncing droplets," Journal of Fluid Mechanics **826**, 97–127 (2017).

[7] Y. Couder, S. Protière, E. Fort, and A. Boudaoud, "Walking and orbiting droplets," Nature **437** (2005).

[8] K. Kumar, "Linear theory of faraday instability in viscous liquids," Proc. R. Soc. A **452**, 1113–1126 (1996).

[9] D. M. Harris and J. W. M. Bush, "Generating uniaxial vibration with an electrodynamic shaker and external air bearing," Journal of Sound and Vibration **334**, 255–269 (2015).

[10] D. M. Harris, J. Quintela, V. Prost, P.-T. Brun, and J. W. M. Bush, "Visualization of hydrodynamic pilot-wave phenomena," Journal of Visualization **20**, 13–15 (2017).

[11] A. U. Oza, R. R. Rosales, and J. W. M. Bush, "A trajectory equation for walking droplets: hydrodynamic pilot-wave theory," J. Fluid Mech. **737**, 552–570 (2013).

[12] M. Labousse, S. Perrard, Y. Couder, and E. Fort, "Build-up of macroscopic eigenstates in a memory-based constrained system," New Journal of Physics **16**, 113027 (2014).

[13] K. M. Kurianski, A. U. Oza, and J. W. Bush, "Simulations of pilot-wave dynamics in a simple harmonic potential," Physical Review Fluids **2**, 113602 (2017).

[14] A. U. Oza, E. Siéfert, D. M. Harris, J. Moláček, and J. W. Bush, "Orbiting pairs of walking droplets: Dynamics and stability," Physical Review Fluids **2**, 053601 (2017).

[15] J. Arbelaiz, A. U. Oza, and J. W. Bush, "Promenading pairs of walking droplets: Dynamics and stability," Physical Review Fluids **3**, 013604 (2018).

[16] A. P. Damiano, P.-T. Brun, D. M. Harris, C. A. Galeano-Rios, and J. W. M. Bush, "Surface topography measurements of the bouncing droplet experiment," Experiments in Fluids **57**, 163 (2016).

[17] D. M. Harris, T. Liu, and J. W. M. Bush, "A low-cost, precise piezoelectric droplet-on-demand generator," Exp. Fluids **56** (2015).

[18] A. Eddi, A. Decelle, E. Fort, and Y. Couder, "Archimedean lattices in the bound states of wave interacting particles," Europhys. Lett. **87** (2009).

[19] G. Pucci, D. M. Harris, L. M. Faria, and J. W. Bush, "Walking droplets interacting with single and double slits," Journal of Fluid Mechanics **835**, 1136–1156 (2018).

[20] F. Dias, A. I. Dyachenko, and V. E. Zakharov, "Theory of weakly damped free-surface flows: A new formulation based on potential flow solutions," Phys. Lett. A **372**, 1297–1302 (2008).

[21] J. Moláček and J. W. M. Bush, "Drops bouncing on a vibrating bath," J. Fluid Mech. **727**, 582–611 (2013).

[22] S. Protière, A. Boudaoud, and Y. Couder, "Particle-wave association on a fluid interface," J. Fluid Mech. **554**, 85–108 (2006).

[23] S. E. Turton, M. M. P. Couchman, and J. W. M. Bush, "A review of the theoretical modeling of walking droplets: towards a generalized pilot-wave framework," Submitted to Chaos.

[24] C. Borghesi, J. Moukhtar, M. Labousee, A. Eddi, E. Fort, and Y. Couder, "The interaction of two walkers: wave-mediated energy and force," Phys. Rev. E **90** (2014).